COMPARISON OF BIFACIAL AND MONOFACIAL LARGE-AREA n-TYPE SI SOLAR CELLS FROM 100 µm THIN WIRE-SAWN WAFERS

Yvonne Schiele, Nils Brinkmann*, Giso Hahn, Barbara Terheiden
University of Konstanz, Department of Physics, P.O. Box 676, 78457 Konstanz, Germany
Phone: +49 (0) 7531 88 4995, Fax: +49 (0) 7531 88 3895, Email: Yvonne.Schiele@uni-konstanz.de
* now with Solexel Inc., Milpitas, USA

ABSTRACT: Reducing wafer thickness provides the most effective potential to lower the production cost of c-Si PV modules. Two thin n-type solar cell concepts are compared in terms of their optical and electrical properties: a monofacial device with a full-area metal surface at the rear which is beneficial in particular to such thin solar cells and a very similar but even better industrially applicable bifacially collecting device.
The monofacial solar cell exhibits a 0.7 mA/cm^2 higher j_{SC} and 9 mV greater V_{OC} due to better light trapping and less recombination. R_{series} and FF discrepancies of both solar cell concepts nearly compensate themselves which is revealed by an R_{series} itemization and FF loss analysis. The independently certified 20.1% efficiency of the monofacial solar cell exceeds that of the bifacial rear junction device by 0.7%$_{abs}$ under one-sided illumination. However, since the bifacial solar cells feature a very high bifaciality of 99.4%, a total power output comparable to a 23.4% efficient monofacial solar cell can be achieved assuming a typical albedo of 20%.
Keywords: bifacial, boron, n-type, selective, silicon, thin wafer

1 INTRODUCTION

Reducing wafer thickness provides the most effective potential to lower the production cost of crystalline silicon PV modules. It is applicable to all kinds of solar cell concepts without inevitably diminishing conversion efficiency [1]. Open circuit voltage V_{OC} and efficiency η can even be enhanced by using thinner wafers provided surface recombination velocity is low enough [2]. Additionally, the required diffusion length of minority carriers in the Si bulk is smaller so that thinner wafers allow a broader range of material quality and resistivity [3].

Within the European project "20 percent efficiency on less than 100 µm thick industrially feasible crystalline silicon solar cells" (20plµs), the entire production chain from wafering to module integration including a mass-production compatible high-yield process for thin solar cells has been developed [4].

In [5], we have for the first time presented >20% efficient 80 µm thin large-area n-type solar cells which have arisen from 100 µm wire-sawn c-Si wafers. The solar cell concept employed features a full-area metal surface at the rear (monofacial) which is beneficial in particular to such thin solar cells whose light path through the wafer is shorter.

A very similar but even better industrially applicable processing sequence results in another solar cell concept: a bifacially collecting device. The difference consists mainly in a finger/busbar grid metal contact at the rear which enables all metal contacts to be screen-printed. Additionally, bifacial modules can generally produce more electricity depending on the albedo of the ground onto which they are mounted. Furthermore, they are applicable to an east-west oriented installation and can therefore contribute to a more evenly distributed solar power generation throughout the day.

In this study, both solar cell concepts, bifacial and monofacial, are compared in terms of their structure and manufacturing, performance and loss mechanisms. Not only conceptually caused optical differences but also typical electrical properties are examined.

2 EXPERIMENT

For manufacturing of the solar cells (Fig. 1) ~110 µm thin wire-sawn n-type Cz-Si wafers (125×125 mm^2, 2 Ωcm resistivity) are processed (Fig. 2).

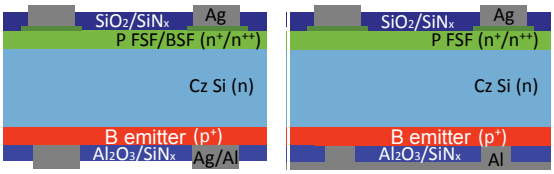

Figure 1: Cross section of the bifacial (left) and monofacial (right) version of the thin n-type Si solar cell.

An initial 55 Ω/sq BBr_3 diffusion after saw damage removal (alkaline texture for bifacial, NaOH bath for monofacial solar cells) and cleaning creates the B emitter which is capped by SiN_x on the rear. An alkaline texture removes the emitter at the front. Subsequently, the wafers are subjected to a $POCl_3$ diffusion creating the FSF/BSF (40 Ω/sq) which is then selectively etched-back (100 Ω/sq) in the non-masked regions between the contact areas (selective n^+ process) [6]. With the rear capping layer removed, the n^+ doped surface is passivated by a stack of thermal SiO_2 and SiN_x, the emitter by an Al_2O_3/SiN_x stack.

The bifacial solar cells are screen-printed on both sides followed by a firing step.

For the monofacial solar cells, only the front Ag grid is screen-printed and fired. Afterwards, the rear passivation is locally opened by means of laser ablation [7], Al is deposited by electron beam evaporation on the full area and finally annealed at low temperatures to cure the electron beam damage [8] and improve the rear contact.

Due to process-related differences, the bifacial solar cell features a final thickness of 100 µm, the monofacial only 80 µm.

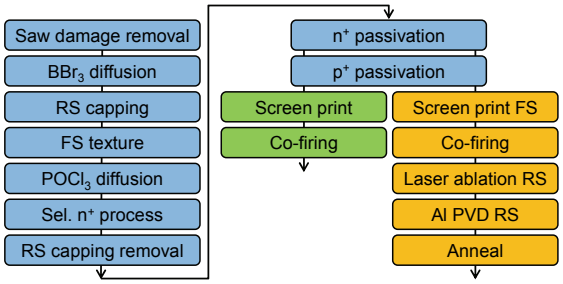

Figure 2: Processing sequence of the bifacial (green) and monofacial (orange) solar cells.

The high-low junction of the solar cells is implemented as a structured doping (sel. n^+ process) in combination with a high level passivation scheme in order to minimize the recombination at the front. To quantify the gain achieved by the n^+ structuring and its special importance to a rear junction device, bifacial solar cells with homogeneous (60 Ω/sq) n^+ field are manufactured as a reference to the selective FSF solar cells and compared under front and rear junction illumination.

3 RESULTS & DISCUSSION

3.1 Front surface field

Compared to a homogeneously n^+ doped layer (60 Ω/sq), the selectively etched-back one implicates a reduction of saturation current density j_{0n+} by ~100 fA/cm^2 with identical passivation stack in the areas between the metal contacts [9]. For the rear junction solar cell, this reduced j_{0FSF} leads mainly to a V_{OC} and j_{SC} rise by 19 mV and 2.2 mA/cm^2 (Tab. I). However, in a front junction concept with an equivalent selective back surface field (BSF), the total η gain is 1%$_{abs}$ less since especially j_{SC} is less impaired by the higher recombination at the rear. This demonstrates that it is essential particularly for rear junction solar cells to minimize the recombination activity at the front which can be implemented by a selectively etched-back FSF in combination with a highly effective passivation layer.

Table I: IV data difference of bifacial solar cells with selective vs. homogeneous n^+ doping ($\Delta X = X_{sel} - X_{hom}$) for rear & front junction illumination.

Illumination type	ΔV_{OC} (mV)	Δj_{SC} (mA/cm^2)	ΔFF (%$_{abs}$)	$\Delta\eta$ (%$_{abs}$)
Rear junction	19	2.2	0.3	1.8
Front junction	17	0.6	0.1	0.8

3.2 Front & rear junction illumination

Illuminating the bifacial solar cell (selective FSF/BSF) from both sides and comparing the absolute values of the IV parameters, the front-junction device features a 0.3 mA/cm^2 higher j_{SC} and a 0.13%$_{abs}$ higher η (Tab. II). The current density gain is mainly attributed to less carrier recombination (PCD measured minority carrier lifetime in the Si bulk $\tau_{bulk} \approx 2$ ms; $L_{eff} \approx 3$ mm from IQE fit) if the emitter is located at the front where the main photon absorption occurs. This is also observed by the slightly enhanced internal quantum efficiency IQE at wavelengths of ~350-800 nm under front junction illumination (Fig. 3).

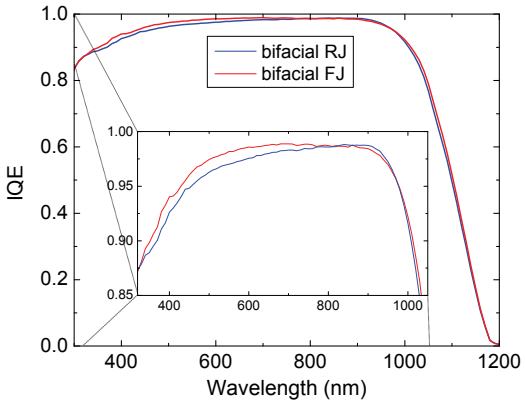

Figure 3: Spectral IQE of the bifacial solar cell for front and rear junction illumination measured with a non-reflecting and non-conducting chuck.

3.3 Bifacial & monofacial solar cell concept

Comparing the IV characteristics of both rear junction solar cell concepts (monofacial and bifacial, Tab. II), it becomes evident that the monofacial solar cell exhibits a 0.7 mA/cm^2 higher short circuit current. The j_{SC} gain is calculated by the difference of the spectral EQE(λ)

$$\Delta j_{SC} = q \cdot \int \phi(\lambda) \cdot \Delta\mathrm{EQE}(\lambda)\mathrm{d}\lambda$$

with elementary charge q and the wavelength dependent photon flux density $\phi(\lambda)$ (Fig. 4).

On the one hand, Δj_{SC} results from an enhanced internal reflectance of the full-area rear PVD-Al layer (Fig. 4). For $\lambda \geq 970$ nm (monofacial) or $\lambda \geq 990$ nm (bifacial), respectively, the absorption length becomes greater than the solar cell thickness causing a steep increase of reflectance. The correspondingly more augmented IQE of the monofacial solar cell exceeds the one of the bifacial although it features a 20 µm smaller wafer thickness (Fig. 4).

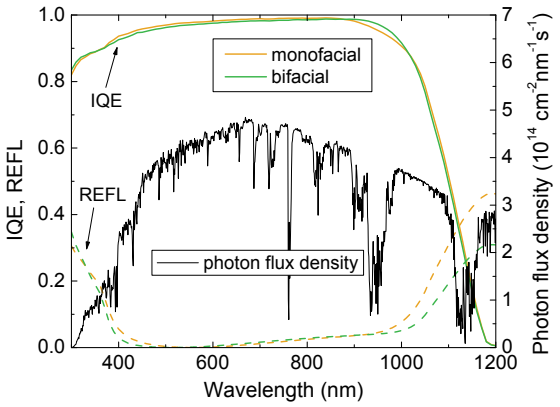

Figure 4: IQE and reflectance of the mono- and bifacial solar cell (non-reflecting, non-conducting chuck) as well as photon flux density of AM1.5g solar spectrum [10].

On the other hand, for $\lambda = 460$-870 nm, the IQE of the monofacial solar cell is above the one of the bifacial, too. This is again caused by the thinner wafer thickness which results in less charge carrier recombination in the Si substrate.

Table II: IV characteristics of the best bifacial and monofacial 5 inch Cz-Si solar cell (in-house measurement on a locally contacting, non-reflecting chuck). The bifacial device is illuminated at the rear or front leading to a front or rear junction solar cell, respectively. R_{series} is determined by the multi-light method, R_{shunt} is calculated from dark IV data, j_{01} and j_{02} from 2-diode model fit.

Solar cell type	V_{OC} (mV)	j_{SC} (mA/cm^2)	FF (%)	η (%)	R_{series} (Ωcm^2)	R_{shunt} (kΩcm^2)	j_{01} (fA/cm^2)	j_{02} (nA/cm^2)
Bifacial FJ	661	37.6	78.44	19.51	0.73	68	115	26
Bifacial RJ	661	37.3	78.54	19.38	0.74	65	128	24
Monofacial RJ	670	38.0	78.56	20.03	0.76	128	110	12

Besides the significantly higher j_{SC}, the monofacial solar cell differs from the bifacial device mainly in terms of the 9 mV higher V_{OC} which is not attributed solely to the j_{SC} increase as this accounts for only $\Delta V_{OC} = 0.8$ mV.

On the one hand, it rather originates from the higher percentage of passivated rear surface due to a smaller metal contact area (~1% laser opening area in monofacial, ~7% Ag/Al metal grid area in bifacial devices).

On the other hand, the evaporated Al annealed at low-temperatures causes less Al spiking than screen-printed and high-temperature fired Ag/Al paste.

Additionally, j_{0e} in the passivated emitter areas of the monofacial solar cell ($j_{0e} \approx 30$ fA/cm^2) is smaller compared to the one of the bifacial device ($j_{0e} \approx 45$ fA/cm^2) due to the non-textured rear surface [9].

These three V_{oc}-increasing effects are also reflected in the 18 fA/cm^2 lower j_{01} (higher passivated emitter surface percentage, smaller j_{0e}) and the halved j_{02} (less Al spiking into the space charge region) of the monofacial solar cell. The less detrimental contact formation of the PVD-Al is also indicated by the shunt resistance R_{shunt} of the monofacial solar cell being twice as great as the one of the bifacial device, even though R_{shunt} is on a very high level for both solar cell types.

R_{series} of the solar cells is composed of the contributions from base, emitter, FSF, contact and metal. The various R_{series} contributions of the mono- and bifacial solar cell type are to be compared:

The contribution of lateral conductivity losses within the emitter to R_{series} (finger distance d_F, finger width W_F)

$$R_{e,LC} = \frac{1}{12} R_{sheet} \cdot (d_F - W_F)^2$$

amounts to 0.23 Ωcm^2 in the bifacial solar cell. In the monofacial device, the spacing of the laser-opened contacts d is only ~10% of the Ag/Al finger distance. However, due to the spot-shaped geometry of the rear contacts, current crowding must be taken into account. In this case, the emitter contribution to R_{series} consists in the spreading resistance [11]

$$R_{e,SR} = \frac{R_{sheet} A_u}{2\pi} [0.25(1 - r_c^4) - (1 - r_c^2) - \ln(r_c)]$$

with r_C being the ratio of contact radius and radius of the unit area A_u from which the contact collects. $R_{e,SR}$ of the monofacial solar cell amounts to 0.003 Ωcm^2. Despite the current crowding, the emitter has no significant influence upon R_{series} of the monofacial solar cell as the contact spacing is very small.

The specific contact resistivity of the bifacial solar cell's screen-printed Ag/Al contacts amounts to $\rho_C = 1.6$ mΩcm^2 (measured by transfer length method, TLM). For PVD-Al, it is $\rho_C = 2.9$ mΩcm^2 [12]. However, the laser treatment modifies the emitter and enhances the contact yielding $\rho_C = 2.0$ mΩcm^2 [13] of the monofacial solar cell. The enhanced contact with Ag/Al paste is caused by larger and deeper Al spike pyramids. According to

$$R_C = \frac{A_u}{A_c} \cdot \rho_C \ ,$$

influenced by the different ratios of contact area A_c and collecting area A_u, the contribution of the emitter-metal contact to R_{series} of the monofacial solar cell amounts to 0.20 Ωcm^2 whereas it is only $R_C = 0.04$ Ωcm^2 for the bifacial.

In the latter, the series resistance contribution of the Ag/Al finger has to be added

$$R_F = \frac{1}{3} R_L \cdot l^2 \cdot (d_F - W_F)$$

with line resistance R_L, effective finger length l resulting in $R_F = 0.08$ Ωcm^2. Since the IV measurement of the solar cells is conducted with a locally contacting chuck (in-house measurement), for the monofacial device an R_{series} contribution of the thin Al layer (thickness d_{Al}) on the rear has to be added as resistance of the rear metal:

$$R_{Al} = \frac{1}{3} \cdot \frac{\rho_{Al}}{d_{Al}} {l_{Al}}^2$$

with specific resistivity ρ_{Al} of the PVD-Al and l_{Al} being the distance to be overcome by the carriers towards the contact pin. R_{Al} amounts to 0.15 Ωcm^2.

In total, the discussed R_{series} contributions differing in both cell concepts sum up to 0.35 Ωcm^2 for both, the mono- and the bifacial device. Due to the 20 µm wafer thickness difference, the bifacial solar cell features an additionally 0.02 Ωcm^2 reduced series resistance, mainly because of a lower contribution of the FSF $R_{FSF,SR}$ (substrate contributes to lateral conductivity). Accordingly, the measured discrepancy of 0.02 Ωcm^2 in R_{series} (Tab. II) is demonstrated.

The combination of all FF influencing parameters (R_{seris}, R_{shunt}, j_{01}, j_{02}) finally results in a nearly identical fill factor FF of both solar cell concepts. This is itemized in a fill factor loss analysis (FFLA) (Fig. 5) [14,5].

The monofacial solar cell features a 0.16%$_{abs}$ higher upper limit of FF being restricted only by j_{01} recombination (sum of measured FF and all losses). The greatest FF loss is caused by R_{series} and is increased by 0.17%$_{abs}$ for the monofacial device. R_{shunt} of both solar cells is high enough to virtually not influence FF (0.01-0.02%$_{abs}$). FF losses due to j_{02} recombination are increased by 0.02%$_{abs}$ for the bifacial counterpart.

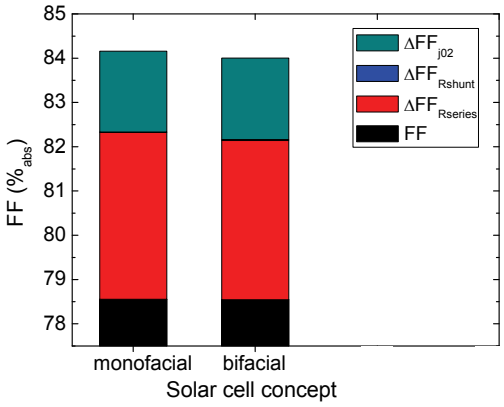

Figure 5: Upper limit of *FF* and *FF* losses according to FFLA for both solar cell concepts.

Mainly due to V_{OC} and j_{SC}, the efficiency of the monofacial solar cell exceeds that of the bifacial rear junction device by 0.65%$_{abs}$. An independently certified measurement (FhG ISE CalLab) of the best cell yields an efficiency of 20.1% being the highest value of a 80 µm thin large-area solar cell from a 100 µm wire-sawn wafer published thus far [5].

However, the manufacturing of the monofacial solar cell is more costly and complex. Despite a lower efficiency of the bifacial device (one-side illumination, measured on a locally contacting, non-reflecting and non-conducting chuck), the total energy output may be higher depending on the albedo. Since the manufactured solar cell features very high bifaciality (η_{RS}/η_{FS}) of 99.4%, a total power output which corresponds to a 23.4% efficient monofacial solar cell is achieved assuming an albedo of 20% (typical albedo of crops, wet sand, meadows [15]).

4 CONCLUSION

Reducing wafer thickness provides the most effective potential in order to reduce the production cost of c-Si PV modules. Two thin large-area Si n-type solar cell concepts have been compared: a monofacial device with a full-area metal surface at the rear which is beneficial particularly to such thin solar cells, and a very similar but better industrially applicable bifacially collecting device.

In both solar cell concepts, a selective FSF is integrated which implicates a j_{0n+} reduction of ~100 fA/cm^2 in the passivated areas. For the use in a rear junction bifacial concept, this causes a significant V_{OC} and j_{SC} increase (19 mV, 2.2 mA/cm^2) yielding an η gain of 1.8%$_{abs}$. In a front junction device, however, this gain is 1%$_{abs}$ less since j_{SC} is less impaired by the higher recombination at the solar cell rear.

Comparing the absolute values of the IV parameters of front and rear junction bifacial solar cells, the front-junction device features a 0.3 mA/cm^2 higher j_{SC} and 0.13%$_{abs}$ higher η which is attributed to less carrier recombination if the emitter is located at the front where the main photon absorption occurs.

The monofacial solar cell exhibits a 0.7 mA/cm^2 higher j_{SC} and 9 mV greater V_{OC}. Its R_{series} is only marginally increased but the less detrimental emitter contact formation causes less recombination which finally results in nearly identical *FF* of both solar cell concepts. The independently certified 20.1% efficiency of the monofacial solar cell exceeds that of the bifacial rear junction device by 0.7%$_{abs}$ under one-sided illumination. However, since the bifacial solar cells feature a very high bifaciality of 99.4%, a total power output comparable to a 23.4% efficient monofacial solar cell can be achieved assuming an albedo of 20%.

5 ACKNOWLEDGEMENTS

The authors would like to thank M. Hofstetter for processing assistance and B. Weber for thin wafer sawing. Part of this work was financially supported by the German Federal Ministry for Economic Affairs and Energy (FKZ 0325581). The financial support for part of this work by the European Commission under FP7, contract number 256695 for the collaborative project “20 percent efficiency on less than 100 µm thick industrially feasible c-Si solar cells” (20plµs) is gratefully acknowledged. The authors are solely responsible for this information and it does not represent the opinion of the European Community. The European Community is not responsible for any use that might be made of the data appearing therein. The content of this publication is the responsibility of the authors.

6 REFERENCES

[1] M. Taguchi, A. Yano, S. Tohoda, K. Matsuyama, Y. Nakamura, T. Nishiwaki, K. Fujita, E. Maruyama, *24.7% record efficiency HIT solar cell on thin silicon wafer*, IEEE J. Photovolt. **4** (2014) 96.

[2] M. Taguchi, Y. Tsunomura, H. Inoue, S. Taira, T. Nakashima, T. Baba, H. Sakata, E. Maruyama, *High-efficiency HIT solar cell on thin (< 100 µm) silicon wafer*, Proc. 24th EU PVSEC (2009) 1690.

[3] Y. Schiele, F. Book, S. Seren, G. Hahn, B. Terheiden, *Screen-printed Al-alloyed rear junction solar cell concept applied to very thin (100 µm) large-area n-type Si wafers*, Energy Procedia **27** (2012) 460.

[4] B. Terheiden T. Ballmann, R. Horbelt, Y. Schiele, S. Seren, J. Ebser, G. Hahn et al., *Manufacturing 100-µm-thick silicon solar cells with efficiencies greater than 20% in a pilot production line,* Phys. Status Solidi A **212** (2015) 13.

[5] Y. Schiele, N. Brinkmann, J. Ebser, R. Horbelt, A. Frey, J. Engelhardt, G. Hahn, B. Terheiden, *>20% efficient* 80 *µm thin industrial-type large-area solar cells from* 100 *µm sawn c-Si wafers*, Proc. 42nd IEEE PVSC (2015), in press.

[6] H. Haverkamp, A. Dastgheib-Shirazi, B. Raabe, F. Book, G. Hahn, *Minimizing the electrical losses on the front side: Development of a selective emitter process from a single diffusion*, Proc. 33rd IEEE PVSC (2008) 430.

[7] J. Engelhardt, A. Frey, L. Mahlstaedt, S. Gloger, G. Hahn, B. Terheiden, *Boron emitters from doped PECVD layers for n-type crystalline silicon solar cells with LCO*, Energy Procedia **55** (2014) 235.

[8] Y. Schiele, G. Hahn. B. Terheiden, *Investigation of radiation damage to the Al_2O_3 / Si wafer interface during electron beam evaporation by means of C-V and lifetime measurements*, Proc. 26th EU PVSEC (2011) 1068.

[9] Y. Schiele, S. Joos, G. Hahn, B. Terheiden, *Etch-back of p^+ structures for selective boron emitters in n-type c-Si solar cells*, Energy Procedia **55** (2014) 295.
[10] IEC 60904-3: *Photovoltaic devices – Part 3: Measurement principles for terrestrial photovoltaic (PV) solar devices with reference spectral irradiance data* (1989).
[11] R.N. Hall, T.J. Soltys, *Polka dot solar cell*, Proc. 14th IEEE PVSC (1980) 550.
[12] Y. Schiele, G. Hahn, B. Terheiden, *Contacting and recombination analysis of boron emitters via etch-back for advanced n-type Si solar cells*, Proc. 29th EU PVSEC (2014) 825.
[13] Y. Schiele, PhD thesis, University of Konstanz, to be published.
[14] A. Khanna, T. Müller, R.A. Stangl, B. Hoex, P.K. Basu, A.G. Aberle, *A fill factor loss analysis method for silicon wafer solar cells*, IEEE J. Photovolt. **3** (2013) 1170.
[15] Wikipedia – The Free Encyclopedia, *Albedo* (http://en.wikipedia.org/wiki/Albedo), Sep. 2015.